Ratchet-driven fluid transport in bounded two-layer films of immiscible liquids

Karin John,[a] Peter Hänggi[b] and Uwe Thiele*[bcd]

We present a two-layer thin film model allowing us to study the behavior of a general class of 'wettability ratchets' that can be employed to transport a continuous phase. Brownian ratchets, in contrast, are normally used to transport particles or molecules within a continuous carrier fluid without transporting the fluid itself.

The wettability ratchet is based on a switchable, spatially asymmetric, periodic interaction of the free surface of the film and the walls. To illustrate the general concept, we focus on an electrical dewetting mechanism based on the effective force exercised by a static electric field on the liquid–liquid interface between two dielectric liquids. In particular, we analyse (i) an on–off ratchet with a constant lateral force resulting in a dewetting–spreading cycle, (ii) a ratchet switching between two shifted potentials that shows a transition between oscillating and sliding drops, and (iii) a flashing external force ratchet. For the three cases, the macroscopic transport is studied in its dependence on spatial and temporal characteristics of the ratchet, and physical properties and volume of the liquids.

1 Introduction

In spatially extended systems without global gradients, transport may be generated by Brownian ratchets.[1–4] Many examples involve particles or molecules in solution that perform a directed net motion in response to the action of the ratchet. There, the ratchet does not induce a mean flow of the solvent itself. For instance, colloidal particles, suspended in solution, move when exposed to a sawtooth electric potential, which is successively turned on and off.[5] A similar concept is employed to selectively filter mesoscopic particles through a micro-fabricated macroporous silicon membrane with etched one-dimensional asymmetrical bottleneck-like pores[6] using an oscillating pressure gradient across the membrane.[7,8] Brownian ratchets are also thought to represent the underlying mechanism of molecular motors that are responsible for the active transport of molecules along filaments in biological cells.[9,3]

The underlying principle of Brownian transport was first pointed out by Curie.[10] He stated that even in a macroscopically symmetric system, macroscopic transport can be induced if the system exhibits local asymmetries *and* is kept out of equilibrium. The local asymmetry can result, for instance, from a periodic but asymmetric potential. The variation has to be on a small length scale as compared to the system size. There are many ways to keep the system out of equilibrium, *e.g.* a chemical reaction,[9] an oscillating pressure[8] or an electric potential that is periodically switched on and off.[5]

[a]*LSP, Université J. Fourier, BP 87 - 38402 Grenoble Cedex, France. E-mail: kjohn@spectro.ujf-grenoble.fr*

[b]*Institut für Physik, Universität Augsburg, D-86135 Augsburg, Germany. E-mail: peter.haenggi@physik.uni-augsburg.de*

[c]*Department of Mathematical Sciences, Loughborough University, Loughborough, Leicestershire, UK LE11 3TU. E-mail: u.thiele@lboro.ac.uk*

[d]*Max-Planck-Institut für Physik komplexer Systeme, Nöthnitzer Str. 38, D-01187 Dresden, Germany. Web: http://www.uwethiele.de*

Most present applications use ratchets to transport or filter discrete objects like colloidal particles or macromolecules. However, ratchets may also serve to induce macroscopic transport of a continuous phase using local gradients only. One example, strongly related to the above cases of particle transport in a 'resting' liquid phase, is the Brownian motion of magnetic particles in ferrofluids when an oscillating magnetic field is applied.[11] In contrast to the above cases, the motion is also transmitted to the liquid solvent by viscous coupling.

Another class of systems does not need colloidal particles to drive the motion of the liquid phase. In a first example, a secondary large scale mean flow is triggered in Marangoni–Bénard convection over a solid substrate with asymmetric grooves.[12] The direction and strength of the mean flow can be controlled by changing the thickness of the liquid layer and the temperature gradient across the layer.

A second example are Leidenfrost drops that are placed on a hot surface with a similar ratchet-like topography. The locally asymmetric geometry induces a directed motion of the drops.[13,14] The effect is observed for many liquids in a wide temperature range in the film-boiling regime.

In a third example, micro-drops confined in the gap between asymmetrically structured plates move when drop shape or wetting properties are periodically changed by different means, like vibrating the substrate, applying an on/off electric field across the gap or a low-frequency electric field of zero mean value along the gap.[15] In a related experiment the motion of drops on a global wettability gradient is strongly enhanced when a periodic force is applied.[16,17] The ratchet aspect is introduced by the intrinsically asymmetric shape and contact angle hysteresis of the drop on the gradient substrate.

Theoretical approaches are very well developed for Brownian ratchets related to particle transport.[3] Detailed studies exist for many ratchet types like drift ratchets,[7] inertia ratchets,[18–20] ratchets with non-coherent switching.[21] However, models for ratchet-driven transport of a continuous phase are a rather

scarce commodity although the concept is thought to be important for emerging microfluidic applications.[22–24]. Ref. 25 proposes a simple electro-osmotic model for liquid flow in a channel induced by locally asymmetric periodic arrays of electrodes under an AC voltage.[26] In this way one can drive an electrolyte depending on the surface properties, *e.g.* capacitance or shape. The redistribution of charges in the Debye-layer leads to an effective electro-osmotic slip velocity at the surface.

In the present work we propose and analyse a model for ratchets related to the third experimental example above that result in a macroscopic transport of a continuous phase. Specifically, we study a model for the flow of two immiscible layered liquids confined between two walls and driven by a flashing 'wettability ratchet'. We employ a rather general concept of wettability comprising all effective interactions between the liquid–liquid free interface and the solid walls. Any such interaction that is applicable in a time-periodic, spatially periodic (but locally asymmetric) way can drive a mean flow, *i.e.* result in transport. We thus extend our previously developed concept for ratchet-driven transport in a single liquid layer bounded by air[27] to a liquid bilayer system confined by the capacitor walls. One major result of this generalized model is the possibility to increase the macroscopic flux in the bottom layer by bounding it with a liquid of low viscosity and large dielectric permittivity instead of air.

There exist several possibilities for an experimental realization of spatially inhomogeneous interactions and switching in time. A simple setup consists of thin films of dielectric liquids in a capacitor with a periodic, locally asymmetric voltage profile, that is periodically switched on and off. A spatially homogeneous electric field destabilizes the interface between the two liquids.[28,29] Initial surface fluctuations with a selected wavenumber are most strongly amplified, resulting in droplet or column patterns that might undergo a coarsening process for large times.[30] This scenario is reminiscent of spinodal dewetting.[31–35] However, the instability is driven by the electrostatic field and not by van der Waals forces. One might call the process electro-dewetting. It is already used to (hierarchically) structure one- or two-layer polymer films.[28,29,36,37] The basic mechanisms are rather well modeled and understood.[28,30,38,39] In particular, the models for bilayer systems on solid substrates with two free interfaces predict a rich interfacial phenomenology like, for instance, the evolution of instabilities with two different wavelengths at the two free interfaces.[39] Similar behavior is also found for a bilayer evolving under the sole influence of effective molecular interactions.[40,41] However, using a spatially heterogeneous electrical field is similar to dewetting on heterogeneous substrates, where a flat film is not only unstable with respect to the spinodal surface instability but also to modes directly driven by the local wettability gradients.[38,42–45] As a result the intrinsic spinodal wavelength and the periodicity of the heterogeneity compete with direct consequences for templating strategies: the heterogeneity is only replicated if its length scale is comparable or slightly larger than the spinodal wavelength.

Fig. 1 sketches an idealized electrical wettability ratchet based on the above discussed effects. Schematically it works as follows. A flat interface between two immiscible liquids that wet the respective walls is stable when the electric field is switched off [Fig. 1 (a)]. When switching on the spatially inhomogeneous

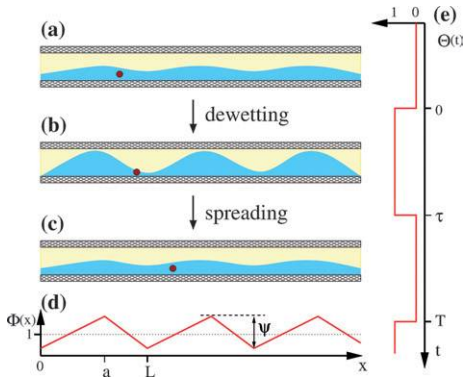

Fig. 1 Panels (a) to (c) illustrate the working principle of a fluidic ratchet based on a switchable wettability profile that causes dewetting–spreading cycles. (d) illustrates the spatial asymmetric periodic interaction profile $\Phi(x)$ responsible for the wettability pattern and (e) indicates the time-dependence $\Theta(t)$ of the switching in relation to the dewetting and spreading phases in (a) to (c). The filled circle indicates a fluid element that is transported during one ratchet cycle although the evolution of the interface profile is exactly time-periodic.

electric field at $t = 0$ [see spatial profile and time-dependence in Fig. 1 (d) and (e), respectively] the films evolve into a set of drops because the interface is destabilized by the overall electric field *and* its local gradients [Fig. 1 (d)]. The latter interfere with the wavelength selection in the linear phase of the surface instability as well as with the coarsening process. Assuming that the lower liquid has the higher relative dielectric constant, the qualitative behavior in this phase of the cycle resembles dewetting of a single film on a substrate with a chemical wettability pattern.[44–46] After transients have died out all the lower liquid is collected in drops situated at the patches of maximal voltage [Fig. 1 (b)]. After switching off the field at $t = \tau$ [defined in Fig. 1 (e)] the drops spread [Fig. 1 (c)] until reaching again the homogeneous two-layer situation [Fig. 1 (a)]. A new cycle restarts a $t = T$ by switching on the field again. If a cycle is not long enough the interface does not become entirely flat, a small modulation remains as indicated in Fig. 1. Note that after initial transients have died out the evolution of the film profile over one cycle is exactly time-periodic. However, the liquid within the layers is redistributed resulting in a mean transport. This is indicated by the changing position of the particle in Fig. 1.

The present paper is structured as follows. In Section 2 we sketch the derivation of the evolution equation for the profile of the interface between two immiscible liquids in a capacitor. Section 3 analyses the basic solution behavior for (i) the homogeneous autonomous system, *i.e.*, the linear stability for a flat interface in a homogeneous static electric field, and (ii) nontrivial steady drop-like states in homogeneous and heterogenous static fields. Section 4.1 simplifies the two-layer equations for the case of a single liquid layer under (passive) air, and extends the corresponding results given in a recent letter.[27] The subsequent Section 4.2 analyses the full two-layer case focusing on the dependencies on experimentally important control parameters. Sections 4.3 and 4.4 then discuss drop transport using two shifted ratchets and transport in symmetric potentials, respectively. The final Section 5 summarizes, compares to the literature and gives an outlook on future work.

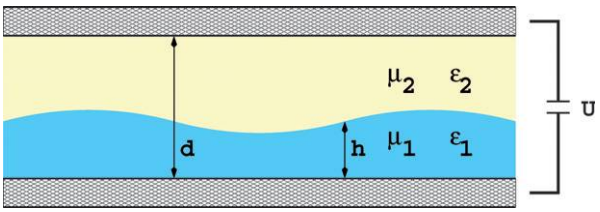

Fig. 2 Sketch of a two-layer film in a capacitor of gap width d and voltage $U(x)$. μ_1 (μ_2) and ε_1 (ε_2) denote the viscosity and relative dielectric constants of the bottom (top) fluid layer, respectively. The thickness of the bottom fluid layer is denoted by $h(x)$.

2 Model

2.1 Evolution equation

We consider two layers of immiscible dielectric fluids between solid smooth walls as sketched in Fig. 2. The liquid–liquid interface is free to move under the influence of capillarity, wettability and an applied electrical field. We present the model for a two-dimensional geometry corresponding to a shallow channel with negligible influence of the lateral side walls.

For the small scale systems considered dominated by wettability and capillarity the dynamics is well described by an evolution equation for the film thickness profile $h(x)$ derived using the lubrication approximation.[47,48] Note, that one can formally use the lubrication approximation only for systems involving small interface slopes. However, in many cases the lubrication approximation predicts the correct qualitative behavior even for partially wetting systems with large contact angles.[47] The derivation from the basic transport equations and boundary conditions performed in analogy to ref. 49 gives

$$\partial_t h = -\partial_x[Q(h)\{\partial_x[\Pi(h,x,t) + \gamma\partial_{xx}h] + f_e(t)\}]. \tag{1}$$

The evolution equation (1) describes the change in time of the interface profile as the negative divergence of the flux in layer 1

$$j_1 = -Q(h)[\partial_x p - f_e(t)] \tag{2}$$

expressed as the product of the mobility and a pressure gradient and/or external force, where the pressure is given by

$$p = -\Pi - \gamma\partial_{xx}h. \tag{3}$$

It contains the curvature pressure $-\gamma\partial_{xx}h$ and the additional disjoining pressure $-\Pi(h,x,t)$. Note that without external force the flux in layer 2, j_2, is given by $j_2 = -j_1$, *i.e.*, there is no net flux through the combined system. The mobility Q is given by

$$Q = \frac{h^3(d-h)^3}{3D}[h\mu_2 + (d-h)\mu_1] \tag{4}$$

with

$$D = \mu_1^2(d-h)^4 + \mu_2^2h^4 + 2\mu_1\mu_2h(d-h)[2h^2 + 3h(d-h) + 2(d-h)^2]. \tag{5}$$

The disjoining pressure $\Pi(h,x,t)$ comprises all effective interactions between the liquid–liquid interface and the walls, *i.e.* the wettability properties.[47,50,51] Here we include the influence of the electrical field obtaining

$$\Pi(h,x,t) = \Psi(x,t)\Pi_{el} + \Pi_{vdW}. \tag{6}$$

For the van der Waals interactions we have

$$\Pi_{vdW} = \frac{1}{6\pi}\left(\frac{A_l}{h^3} + \frac{A_u}{(d-h)^3}\right) \tag{7}$$

Assuming that each liquid wets the adjacent wall better than the other one, the Hamaker constants are $A_l > 0$ and $A_u < 0$. Films of a dielectric liquid in a capacitor with an applied voltage U_0 are subject to the electric pressure[28,30]

$$\Pi_{el} = \frac{1}{2}\varepsilon_0\varepsilon_1\varepsilon_2U_0^2\frac{(\varepsilon_1-\varepsilon_2)}{[\varepsilon_2h + (d-h)\varepsilon_1]^2} \tag{8}$$

For the considered ratchet the electric pressure is modulated in space and time by the function $\Psi(x, t)$. Here, ε_0 is the absolute dielectric constant, whereas ε_1 and ε_2 are defined in Fig. 2.

The external force $f_e(t)$ that depends on time acts parallel to the walls. Simple mechanical realizations of f_e are an inclined system or centrifugal forces yielding an $f_e(t)$ independent of the film thickness and the position x along the walls. Other realizations include thermal or wettability gradients.

For the time-dependence of $\Psi(x,t)$ we will only consider instantaneous switches between two different space dependencies, *i.e.*, for one temporal (flashing) period T we impose

$$\Psi(x,t) = \begin{cases} \Phi_1(x), & 0 \le t < \tau \\ \Phi_2(x), & \tau \le t < T \end{cases} \tag{9}$$

The spatial dependencies Φ_i are assumed to be periodic in x, but break the reflection symmetry in x. In particular, we take the potentials in state 1 and 2 to be piecewise linear asymmetric sawtooth potentials. For one spatial period L we have

$$\Phi_i(x) = \begin{cases} \varphi_i{}^2\left[1 + \frac{\psi_i}{a}\left(x - \frac{a}{2}\right)\right], & 0 \le x < a, \\ \varphi_i{}^2\left[1 - \frac{\psi_i}{L-a}\left(x - \frac{L+a}{2}\right)\right], & a \le x < L\,, \end{cases} \tag{10}$$

where by substituting $x = x' - \Delta x_i$ one can introduce a shift of the ratchet potential by Δx_i along the walls. This setup ensures $(1/L)\int_0^L \Phi_i(x)\,dx = \varphi_i^2$. An example for $\Phi_i(x)$ is shown in Fig. 1 (d). In the present work we shall consider three simple settings:

(i) An on–off ratchet with a constant lateral force f_e and $\phi_2 = 0$, *i.e.*, in phase 2 the electrical field is completely switched off and only van der Waal forces govern the film evolution. In this case one can write $\Psi(x,t) = \Theta(t)\Phi_1(x)$ with the time-dependence [see Fig. 1 (e)]

$$\Theta(t) = \begin{cases} 1, & 0 \le t < \tau \\ 0, & \tau \le t < T. \end{cases} \tag{11}$$

Furthermore, we choose in eqn (10) $\varphi_1 = 1$, $\Delta x_1 = 0$ and $\psi_1 \equiv \psi \neq 0$, *i.e.*, the average voltage is given by $U_0\tau/T$.

(ii) A switching between two potentials of the form of eqn (10) that are translated in space with respect to each other by half a period. We choose $\varphi_1 = \varphi_2 = 1$, $\Delta x_1 = 0$, $\Delta x_2 = L/2$ and $\psi_1 = \psi_2 \equiv \psi \neq 0$. In consequence, the average voltage is U_0. The external force f_e is constant.

(iii) A time-independent symmetric periodic potential $\Psi(x)$ combined with an external force that is switched periodically in time. In particular, we choose in eqn (10) $\varphi_1 = \varphi_2 = 1$, $\Delta x_1 = \Delta x_2 = 0$, $a = L/2$ and $\psi_1 = \psi_2 = 0$. The temporal switching of the external force is

$$f_e = \begin{cases} \bar{f}_e/\sqrt{\theta}, & 0 \le t < \tau \\ -\bar{f}_e\sqrt{\theta}, & \tau \le t < T \end{cases} \tag{12}$$

with θ defined below in eqn (14) corresponding to a zero mean force, *i.e.*, $\int_0^T f_e \mathrm{d}t = 0$. The measure $\bar{f}_e$ used in the following to characterize the strength of the applied force denotes the root-mean-square (RMS) average of the external force, *i.e.*, $\bar{f}_e = [(1/T)\ \int_0^T f_e^2 \mathrm{d}t]^{1/2}$

The ratchets are characterized by use of two measures, namely the asymmetry ratio

$$\phi = \frac{a}{L-a} \tag{13}$$

of the spatial variation $\Phi_i(x)$ and the flashing ratio

$$\theta = \frac{\tau}{T-\tau} \tag{14}$$

of the temporal switching. In the absence of external forces in each layer zero net transport is expected for a symmetrical ratchet, *i.e.*, for $\phi = 1$. For $\phi \neq 1$ the flashing ratchet generates a flow. We quantify the resulting transport by the mean flow of liquid 1

$$\bar{j}_1 = (1/TL)\int_0^T \mathrm{d}t \int_0^L \mathrm{d}x\, j_1(x,t). \tag{15}$$

To obtain a minimal set of parameters we introduce the scales $3\gamma\mu_s/d\kappa^2_{el}$, $\sqrt{\gamma d/\kappa_{el}}$, and d for time t, lateral length x, and vertical length h (and d), respectively. An electrostatic 'spreading coefficient' is defined as $\kappa_{el} = \varepsilon_0\varepsilon_s U_0^2/2d^2$ and we introduce $\varepsilon_s = \varepsilon_1 + \varepsilon_2$, $\mu_s = \mu_1 + \mu_2$, $\varepsilon = \varepsilon_1/\varepsilon_s$ and $\mu = \mu_1/\mu_s$. For simplicity we assume $A_u = -A_l$ and obtain the dimensionless Hamaker constant $A = A_l/6\pi d^3\kappa_{el}$. The scale for the external force is $\sqrt{\gamma d/\kappa^3_{el}}$. Using identical symbols as before, the resulting dimensionless evolution equation reads:

$$\partial_t h = -\partial_x[Q(h)\{\partial_x[\Pi(h,x,t) + \partial_{xx}h] + f_e(t)\}] \tag{16}$$

supplemented with eqn (6). The mobility Q is given by eqn (4) and (5) replacing $\mu_1 \to \mu$, $\mu_2 \to 1-\mu$ and $d \to 1$. The dimensionless van der Waals disjoining pressure is

$$\Pi_{vdW} = A\left[\frac{1}{h^3} - \frac{1}{(1-h)^3}\right] \tag{17}$$

whereas the dimensionless electric pressure is obtained by replacing $\varepsilon_1 \to \varepsilon$, $\varepsilon_2 \to 1-\varepsilon$ and $d \to 1$ in eqn (8) giving

$$\Pi_{el} = \frac{\varepsilon(1-\varepsilon)(2\varepsilon-1)}{[\varepsilon(1-h)+(1-\varepsilon)h]^2} \tag{18}$$

All results are given in dimensionless quantities. Note that the chosen scaling keeps the 'up–down' symmetry of the system under the transformation $h \to 1-h$, $\varepsilon \to 1-\varepsilon$ and $\mu \to 1-\mu$. This symmetry of the equations reflects the fact that an exchange of the two fluids does not alter the dynamics of the system. Note however, that an inclusion of gravity for thick films would break the symmetry.

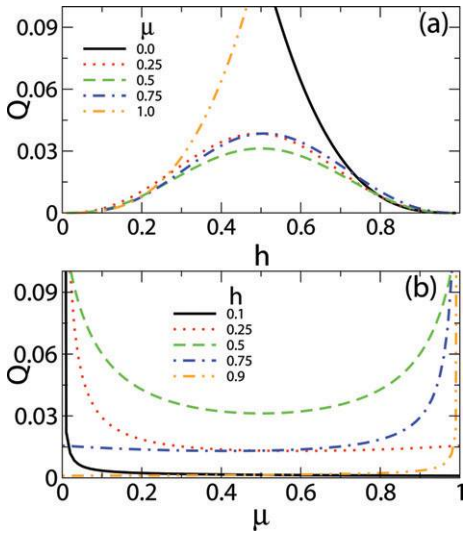

Fig. 3 Dependence of the mobility [eqn (4)] (a) on the film thickness for various viscosity ratios (see legend), and (b) on the viscosity ratio for various film thicknesses (see legend).

2.2 Mobility

The mobility Q of a two-layer system differs from the simple h^3 dependence known from a one-layer system.[47] As shown in Fig. 3 (a) for true two-layer systems ($0 < \mu < 1$) the mobility depends non-monotonically on the film thickness, approaching zero for $h \to 0$ and also for $h \to 1$. As μ approaches 0 or 1, the system effectively becomes a one-layer system and correspondingly the mobility takes the values $(1-h)^3$ and h^3, respectively. For a fixed film thickness the viscosity ratio μ influences the mobility and therefore the time scale of the flow as indicated in Fig. 3 (b). For intermediate values of μ we observe a competition between the influence of the film thickness and the viscosity ratio. For a small film thickness h the effect of viscosity on mobility becomes very strong for small μ, whereas for large h this effect

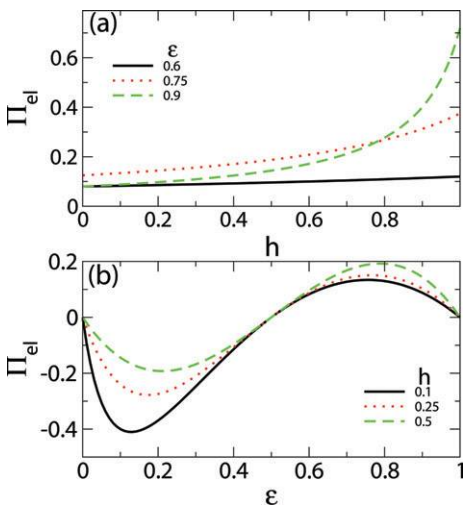

Fig. 4 Dependence of the electric disjoining pressure [eqn (18)] (a) on the film thickness for various permittivity ratios (see legend), and (b) on the permittivity ratio for various film thicknesses (see legend).

is observed for large μ reflecting the above discussed 'up-down' symmetry.

2.3 Electric disjoining pressure

Fig. 4 depicts the dependence of the disjoining pressure on the film thickness and the permittivity ratio. For $\varepsilon > 0.5$ the disjoining pressure monotonically increases with increasing film thickness. The dependence of Π_{el} on the permittivity ratio for a fixed film thickness is non-monotonic, possessing a maximum and a minimum at $\varepsilon > 0.5$ and $\varepsilon < 0.5$, respectively. Furthermore Π_{el} switches sign at $\varepsilon = 0.5$.

2.4 Efficiency measure

To evaluate the feasibility of the 'wettability ratchet' for applications it is very important to determine its capacity to transport liquid against an external force. In the absence of macroscopic forces no work is performed and all energy is lost *via* viscous dissipation. This is not the case for a thin film ratchet under load, *i.e.* $f_e \neq 0$ in eqn (16). Switching off the ratchet, $f_e < 0$ induces a macroscopic film flow in negative direction.

We define an efficiency measure following the reasoning for a ratchet in the overdamped regime given in ref. 9. In particular, the transport under load is characterized by the (mechanical) energy transport efficiency

$$\nu_{\text{eff}} = -\frac{\dot{W}_m}{\dot{W}_d} \tag{19}$$

where

$$\dot{W}_m = \frac{1}{TL}\int_0^L \mathrm{d}x \int_0^T \mathrm{d}t\, (j_1 + j_2)\, f_e \tag{20}$$

and

$$\dot{W}_d = -\frac{1}{TL}\int_0^L \mathrm{d}x \int_0^T \mathrm{d}t\, (j_1 - j_2)\, \partial_x p \tag{21}$$

represent the mechanical work performed and the interaction energy consumed per unit time, respectively.

Note that following ref. 52–54 one can define the alternative efficiency measure:

$$\tilde{\nu}_{\text{eff}} = -\frac{\bar{j}_1\, (-\overline{\partial_x p} + f_e) + \bar{j}_2\, (\overline{\partial_x p} + f_e)}{\dot{W}_d} \tag{22}$$

where $\dot{W}_d$ denotes the total dissipation per unit time as before and

$$\overline{\partial_x p} = \frac{1}{TL}\int_0^T \mathrm{d}t \int_0^L \mathrm{d}x\, \partial_x p \tag{23}$$

Performing the integration in eqn (23) using periodic boundaries in x, we obtain $\overline{\partial_x p} = 0$ and the two definitions eqn (19) and eqn (22) coincide. For the one-layer case we simply neglect dissipation in the gas phase and set $j_2 = 0$.

3 Time-independent potentials

Before we embark on the analysis of the proposed electric wettability ratchets we present in Sections 3.1 and 3.2 basic results for time-independent, spatially homogeneous and inhomogeneous potentials, respectively. This will allow us to better understand the conditions of maximal flux through the fluid ratchet.

Thereby, all steady state solutions are calculated using continuation methods.[55–57] The latter were recently applied to thin film models, for instance, in the context of sliding drops,[58,59] chemically driven running drops,[60] depinning drops on heterogeneous substrates,[61] and open two-layer films.[40,62]

3.1 Homogeneous system

To study the film behavior for time-independent, spatially homogeneous potentials we fix $\Psi(x,t) \equiv 1$ and $A = 0.001$. First, we determine the stability of flat films, *i.e.* the spinodal and binodal lines,[63–65] in the parameter space spanned by the mean film thickness $\bar{h}$ and the permittivity ε. Both are given in Fig. 5 for the two unstable regions found for $\varepsilon > 1/2$ and $\varepsilon < 1/2$, respectively. As before, the 'up–down' symmetry is reflected by the invariance under the transformation $\varepsilon \to 1 - \varepsilon$ and $\bar{h} \to 1 - \bar{h}$. For $\varepsilon = 1/2$ the system is stable, since the two fluids have identical electrical properties and the resulting electrostatic force is zero. For $\varepsilon = 0$ and $\varepsilon = 1$, the permittivity contrast of the two layers becomes infinite, *i.e.*, the limit does not correspond to a physical situation. For values of ε close to the stable configuration the destabilizing electrostatic forces are very weak and the van der Waals interactions stabilize even micrometric films. Note however, that for macroscopic films, the stable region becomes very small. In the spinodal region the film is linearly unstable, *i.e.* infinitely small perturbations grow exponentially in time. The linear modes can be determined by linearizing eqn (1) with respect to small harmonic perturbations of a homogeneous flat film of thickness h. One obtains the dispersion relation

$$\beta = Q(h)k^2(\partial_h \Pi - k^2) \tag{24}$$

where β and k are the growth rate and the wavenumber of the harmonic perturbation, respectively. The maximum of the dispersion relation at

$$k_m = \sqrt{\frac{1}{2}\partial_h \Pi} \tag{25}$$

corresponds to the fastest growing unstable mode. Fig. 6(a) and (b) give k_m and the corresponding growth rate $\beta_m = Q(h)k_m^4/4$,

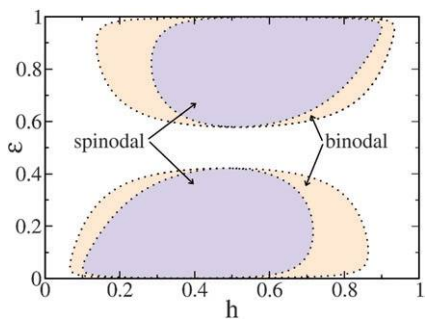

Fig. 5 Linear and absolute stability of the flat liquid–liquid interface for a two-layer system in a capacitor. The system is unstable with respect to infinitely small (finite) perturbations in the regions labeled spinodal (binodal) and stable otherwise. The remaining free parameter is $A = 0.001$.

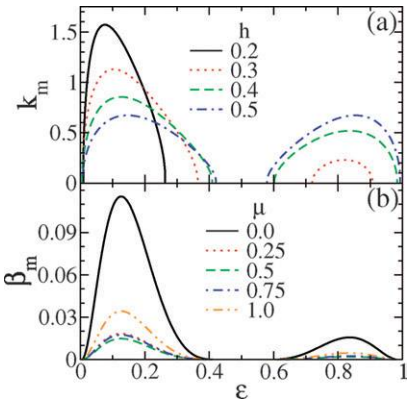

Fig. 6 Shown are (a) the wavenumber and (b) the growth rate of the fastest growing linear mode as functions of the permittivity ε for several film thicknesses h as given in the legend. The film thickness in (b) is $h = 0.4$. The remaining parameter is $A = 0.001$.

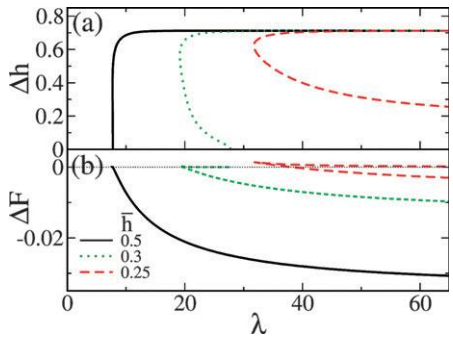

Fig. 7 Steady drop solutions in a capacitor with spatially homogeneous voltage. Shown are the dependencies of (a) the amplitude Δh and (b) the energy difference ΔF on the period λ (*i.e.* a measure of droplet size) for various $\bar{h}$ as given in the legend. The remaining parameters are $A = 0.001$ and $\varepsilon = 0.75$.

respectively, for several choices of parameters indicating the strong dependence of the spatial scale and growth rate on the permittivity ratio and the film thickness. In contrast to the spinodal region, to 'rupture' a film in the binodal region requires finite disturbances that exceed an unstable threshold or nucleation solution. This region is not studied here (but see in this context ref. 64,65).

In the spinodal region, as soon as the electrical field is applied, all unstable harmonic modes start to grow exponentially; the one with the fastest growth rate dominates. However, at larger amplitudes the nonlinear terms of eqn (1) become important. They might either accelerate or slow down the evolution in time, depending on the specific parameter values. For van der Waals forces as chosen here, the short-time evolution finally saturates and the profile approaches steady state solutions. These are, however, on a larger time scale unstable to coarsening. Fig. 7 (a) presents families of steady state solutions obtained by continuation[57] for a fixed permittivity contrast ε. The steady state solutions can be further characterized by the difference ΔF of their energy and the energy of the flat film, *i.e.*, $\Delta F = (1/L) \int_0^L \mathrm{d}x\, f[h(x)]$ where the energy density f is given by

$$f = \frac{1}{2}(\partial_x h)^2 - \int_{\bar{h}}^{h} \Pi(h)\, \mathrm{d}h \qquad (26)$$

It can be clearly seen in Fig. 7 (b) that the energy of the system decreases with increasing period, due the reduced cost of the gradient terms. Note that unstable nucleation solutions are characterized by $\Delta F > 0$. In the next section basic results are given for steady drop solutions for a capacitor with a space-dependent voltage.

3.2 Heterogeneous system

The solution behavior is strongly influenced by heterogeneous walls as intensively studied for dewetting on substrates with wettability patterns. Beside simulations of the time evolution[45,46,66,67] detailed results are available for the steady states.[44,45,68]

We apply the techniques used in ref. 45 to the two-layer system with a heterogeneous voltage. Fig. 8 presents characteristics of selected steady solutions *versus* the amplitude ψ of the heterogeneity. For small values of ψ we find at least three solutions for a fixed heterogeneity period. The one with the lowest energy corresponds to the equilibrium solution. Fig. 9 gives the form

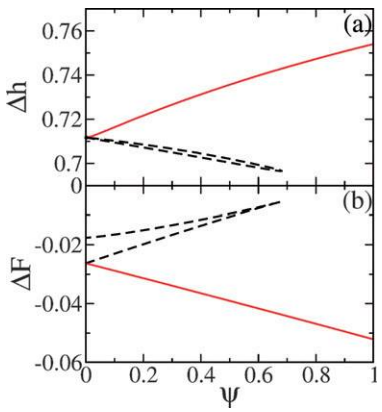

Fig. 8 Dependencies of (a) amplitude Δh and (b) energy ΔF of the steady solutions on the ratchet amplitude ψ. The remaining parameters are $\bar{h} = 0.5$, $\varepsilon = 0.75$, $A = 0.001$, $\phi = 5$, and $L = 32$. The dashed and solid lines denote linearly unstable and stable solutions, respectively.

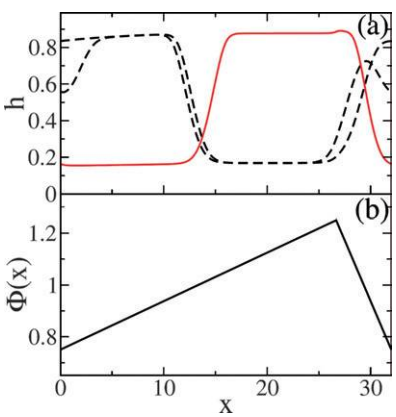

Fig. 9 (a) Selected steady interface profiles and (b) the applied ratchet potential corresponding to Fig. 8.

of the heterogeneity and the interface profiles for the three steady state solutions existing for one set of parameter values. For $\varepsilon > 0.5$, the liquid with higher permittivity is at the bottom (*e.g.* silicon oil on water) and thus the equilibrium solution with the lowest energy represents a drop of the lower liquid sitting at the point of maximal voltage.

4 Results for ratchet systems

In the following we analyse the three proposed specific ratchet types. Sections 4.1 and 4.2 focus on type (i) ratchets in one-layer and two-layer settings, respectively. The alternative ratchet types (ii) and (iii) are investigated in Sections 4.3 and 4.4, respectively.

To numerically study the time-dependent ratchet behavior governed by the dimensionless equations given above in Section 2.1, we employ a Runge–Kutta scheme with adaptive stepsize control and with periodic boundary conditions.[69] Typically, the system was initialized from a flat film solution with small amplitude perturbations. Then the evolution is followed until initial transients have decayed and the system has settled onto a time-periodic cycle whose period corresponds to the switching period T of the ratchet. Such an 'equilibrated cycle' is then used to determine the mean flux per cycle. If not stated otherwise, a unique value is obtained for each parameter set, independent of the initialization of the ratchet and, indeed, the starting configuration.

4.1 One-layer type (i) ratchet

The two-layer model can be simplified assuming that the upper fluid is a passive *gas*, *i.e.* $\mu_2 = 0$ and $\varepsilon_2 = 1$, leading to $\mu \to 1$ and $\varepsilon \geq 1/2$ in the non-dimensional form of the model. The physical scales are adapted by letting $\mu_s \to \mu_1$. The resulting film evolution equation has an identical form to eqn (16) but with $Q(h) = h^3$. The dimensionless pressures Π_{vdW} and Π_{el} are given by eqn (17) and (18), respectively. The system corresponds to the one-layer ratchet model recently presented in ref. 27. In one-layer systems one observes a true overall transport of fluid characterized by the mean flux $\bar{j}_1$.

Fig. 10 shows typical examples of the film evolution during one ratchet cycle for different cycle lengths T and a fixed flashing ratio θ. With an interaction profile $\Phi(x)$ shaped like a sawtooth skewed to the right [Fig. 1 (d)], each cycle transports liquid to the right. With increasing T the evolution becomes more complex. Fig. 10 (c) allows one to distinguish four phases: (1) when the ratchet is switched on the film is nearly flat but rapidly evolves a surface instability with a wavelength given approximately by the corresponding spinodal length. (2) Next, the evolving profile coarsens in two steps, accelerated by the gradients of the ratchet potential. (3) In an ideal situation only one drop remains, corresponding to the equilibrium structure of the heterogeneous wettability pattern produced by the ratchet potential (*cf.* Fig. 9). (4) Finally, after switching off the ratchet, the drop spreads rapidly under the influence of van der Waals forces until the next cycle starts.

For a shorter cycle length [Fig. 10 (b)] there is no time left for the second coarsening step to occur as observed in Fig. 10 (c). For an even shorter period [Fig. 10 (a)] the relaxation without the electric field (spreading) is not fast enough to reach a nearly flat film at the end of the cycle. In consequence, the evolution does not start with the fastest flat film modes but already with a mode of system size, *i.e.*, no coarsening is necessary.

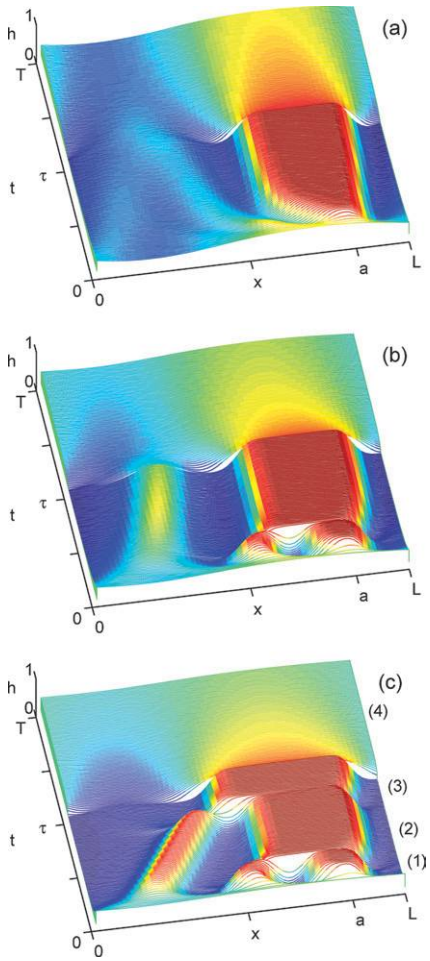

Fig. 10 Space–time plots for one temporal period of the evolution of the film thickness profile for a one-layer film of dielectric liquid in a capacitor [type (i) ratchet]. Shown is one spatial period during one ratchet cycle of cycle length (a) $T = 1000$, (b) $T = 3000$, and (c) $T = 6000$, and fixed flashing ratio $\theta = 1$. The remaining parameters are $\bar{h} = 0.5$, $\psi = 0.5$, $L = 32$, $\phi = 5$, $A = 0.001$, $\varepsilon = 0.75$, $\mu = 1$ and $f_e = 0$. The different phases (1)–(4) indicated in the right of panel (c) are explained in the main text. The starting time is well after initial transients have decayed.

The competing influence of the various parameters allows one to tune the transport properties by adjusting the relative importance of the phases (1) to (4). As indicated by Fig. 11 the transport is strongest for intermediate film thicknesses. However, a film of intermediate thickness in a homogeneous electric field [$\Phi(x) = \Theta(t) = 1$] dewets spinodally with a wavelength well below the spatial period of the ratchet (*cf.* Fig. 6). Therefore, the ongoing coarsening interacts with the flow induced by the spatial asymmetry and leads to a nontrivial dependence of the mean flux on the film thickness. For very small or large film thicknesses the stabilizing van der Waals terms are dominating and the mean flux thus rapidly approaches zero. Note also the flow reversal, albeit with a small mean flux, for large $\bar{h} \gtrsim 0.85$. Further calculations (not shown) demonstrate the monotonic increase of the mean flux with increasing asymmetry ratio ϕ or

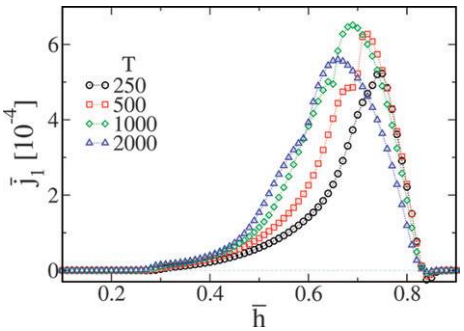

Fig. 11 Dependence of the mean flux $\bar{j}_1$ on the mean film thickness in the capacitor for various flashing periods T as indicated in the legend [one-layer type (i) ratchet]. The remaining parameters are as in Fig. 10.

amplitude ψ of the ratchet potential, with other parameters held constant.

The flashing characteristics of the ratchet have a very pronounced effect on the transport. Fig. 12 (a) depicts the non-monotonic dependence of the flow on the flashing ratio θ and period T, respectively. For small θ the flow is practically zero, since the time for dewetting is too short to trap a considerable amount of liquid at the spots of high wettability. Increasing θ increases the flux until it reaches a maximum at $\theta \approx 1$. Beyond the maximum the flow decreases because less and less time remains for the spreading.

The dependence of the flow on the flashing period T, shown in Fig. 12 (b), gives a similar overall impression. However, around the maximum of the flow one notes a particularly interesting non-monotonic behavior that is related to coarsening. For small periods the fluid has neither enough time to dewet nor to spread and the resulting mean transport is small. For large periods both processes reach the respective equilibrium structure well before the next switching, *i.e.* most time is spend waiting and the mean velocity decreases approximately as $1/T$.

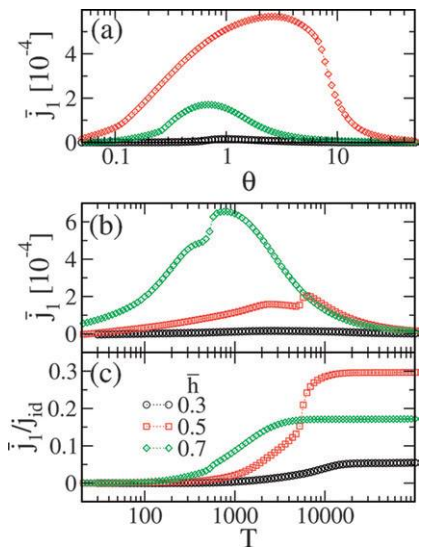

Fig. 12 Dependence of the mean flux $\bar{j}_1$ on (a) the flashing ratio θ (for $T = 2000$) and (b, c) the flashing period T (for $\theta = 1$) for various film thicknesses as given in the legend [one-layer type (i) ratchet]. Panel (c) gives the ratio of the observed mean flux compared to the flux in an ideal ratchet as explained in the main text. The remaining parameters are as in Fig. 10.

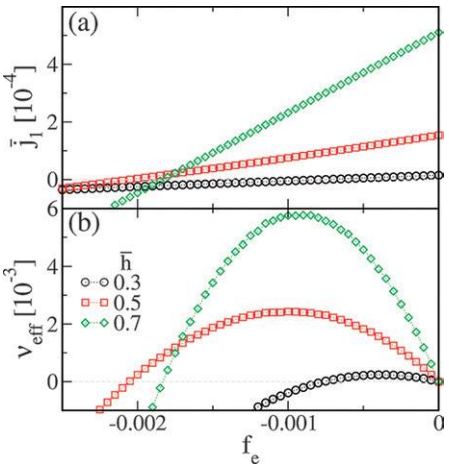

Fig. 13 The influence of an external load, *i.e.*, the lateral force f_e on (a) the mean flux $\bar{j}_1$ and (b) the transport efficiency ν_{eff} for various mean film thicknesses $\bar{h}$ as indicated in the legend [one-layer type (i) ratchet]. The remaining parameters are as in Fig. 10 except for $T = 500$.

The numerical results can be compared to estimates of the flux assuming an idealized setting, *i.e.*, an ideal combination of ratchet properties and intrinsic length and time scales. Approximating the intermediate drops at the maximum of the electrical field as point-like objects, in one cycle of length T all the liquid moves by $a - L/2$. For a film of mean thickness $\bar{h}$ this implies a mean flow of $\bar{j}_{id} = \bar{h}\,(a - L/2)/T$, *i.e.*, the mean velocity is $\bar{v}_{id} = (a - L/2)/T$. The maximal spatial asymmetry is given by $a = L$, *i.e.* $\bar{j}_{max} = \bar{h}L/2T$ and $\bar{v}_{max} = L/2T$. In a real system, however, several effects keep the mean velocity below the ideal value. As a demonstration, Fig. 12 (c) shows the ratio of the numerically determined flux through a realistic ratchet and the idealized ratchet. For optimal parameters in simulations we reach about 30% of $\bar{j}_{id}$ for $\bar{h} = 0.5$ and $T \approx 10\,000$.

The mean flux and transport efficiency are shown in Fig. 13 (a) and (b). To obtain an impression of the physical scale, note that the force scale used for water is 1×10^7 N m^{-3}. The transport efficiency behaves non-monotonically. It increases for small loads, reaches a maximum and decreases for larger loads. It becomes negative when the flow reverses. In the latter case the ratchet does not perform work against the external force.

4.2 Two-layer type (i) ratchet

Next we investigate the transport for the full two-layer system with a non-vanishing viscosity in the top layer depending on various parameters. To characterize the transport properties we calculate the mean flux in layer 1 (positive when directed to the right). In the absence of an external lateral force the net transport summed over both layers is always zero. However, the average flows in the individual layers are finite in an asymmetric ratchet setup. They flow into opposite directions—an ideal setting for applications involving mass transfer.

Fig. 14 shows the dependence of the flux on the mean interface position, *i.e.*, mean film thickness of the lower layer, for various viscosity ratios and a fixed permittivity ratio. One finds a broad optimum for the flux situated roughly between $0.4 < \bar{h} < 0.7$. It indicates that for a small viscosity contrast between the two

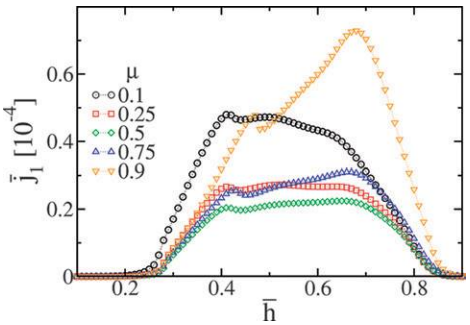

Fig. 14 The dependence of the mean flux on the mean film thickness $\bar{h}$ for various viscosity ratios μ as indicated in the legend [two-layer type (i) ratchet]. The remaining parameters are as in Fig. 10 with $T = 2000$.

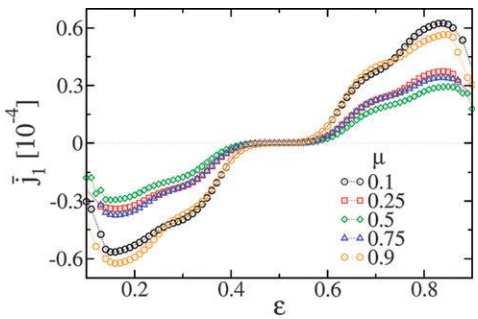

Fig. 15 The dependence of the mean flux on the permittivity ratio ε for different viscosity ratios as indicated in the legend [two-layer type (i) ratchet]. The remaining parameters are as in Fig. 10 with $T = 2000$.

fluids ($0.25 < \mu < 0.75$) the flow is relatively independent of the film thickness. For small $\mu = 0.1$ the same holds true but with a larger optimal flux. However for large $\mu = 0.9$ ($\mu_1 \gg \mu_2$) the flux exhibits a pronounced maximum at $\bar{h} \approx 0.7$. This maximum is a result of the competition between an increase in the mean electric disjoining pressure for increasing $\bar{h}$ and a parallel decrease in the mobility. The latter results from filling up the gap with the more viscous liquid.

Fig. 15 depicts the dependence of the flux on the permittivity ratio ε for the case where the capacitor is filled with the two liquids in equal parts ($\bar{h} = 0.5$). Direction and magnitude of the flux strongly depends on ε. Keeping the sum of the relative permittivity ratios, ε_s, constant (corresponding to a fixed time scale) flow extrema for flow in opposite directions are found at about $\varepsilon = 0.15$ and $\varepsilon = 0.85$, respectively. For similar permittivities of the two liquids the flux approaches zero. The flux reversal occurs precisely at $\varepsilon = 0.5$.

The dependence of the average flux on the viscosity ratio μ (not shown) does not exhibit any unexpected features. It essentially follows the dependence of the mobility on μ given above in Fig. 4.

As for the one-layer system we also investigated the dependence of the flow on the flashing period and the flashing ratio (not shown). The behavior resembles that of the one-layer system shown in Fig. 12. For a fixed flashing ratio $\theta = 1$ the optimal flux regime occurs at $T \approx 10^3 \ldots 10^4$ depending on the particular viscosity contrast. The optimal flux is lowest for a small viscosity contrast ($\mu \approx 1/2$) and is also shifted towards larger flashing periods. Accordingly, the flux depends non-monotonically on the flashing ratio. For small θ the magnitude of the mean flux increases with increasing θ until it goes through a maximum at values $0.1 < \theta < 1$ depending on the viscosity contrast and then decreases with increasing θ. The optimal flux for a small viscosity contrast is shifted towards lower flashing ratios and has a magnitude considerably lower than for a high viscosity contrast.

4.3 Droplet transport in a type (ii) ratchet

The transport with a type (i) flashing ratchet discussed up to here relies on a deterministic phase (ratchet on, dewetting) and a subsequent diffusive phase (ratchet off, spreading). This setting already guarantees a reliable transport with a relatively small exposure of the liquid to the electric field, since the flux maximum occurs at a flashing ratio where the ratchet is actually off most of the time. However, if heating of the liquid does not pose a problem, one might increase the transport efficiency by switching between spatially shifted ratchet potentials [type (ii) ratchet, *cf.* Section 2.1]. A further advantage of a type (ii) ratchet

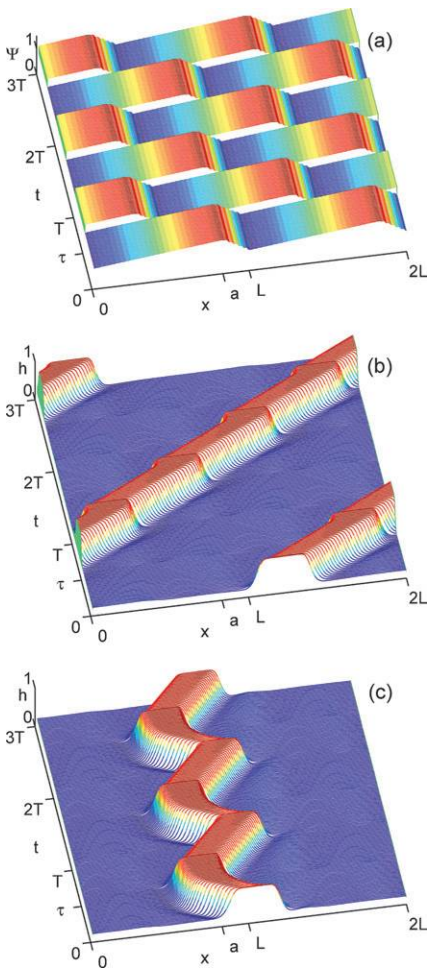

Fig. 16 Transport of entire droplets using a type (ii) ratchet consisting of two temporally and spatially shifted ratchet potentials. Different flashing periods result in qualitatively different behavior. Shown are (a) the ratchet potential and the film thickness for (b) $T = 6000$, and (c) $T = 3000$. The remaining parameters are $L = 32$, $\mu = 1$, $\varepsilon = 0.75$, $A = 0.001$, $\bar{h} = 0.3$, $\psi = 0.5$, $\Delta x = L/2$, $\phi = 5$, $\theta = 1$, and $f_e = 0$.

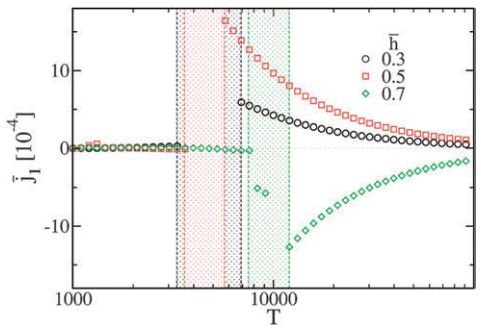

Fig. 17 Flux depending on the flashing period for two alternating ratchet potentials [type (ii) ratchet] for various film thicknesses as indicated in the legend. The transition from zero to high flux is accompanied by a non-stationary flux regime marked by the shaded region between the thin dashed lines. The parameters are as in Fig. 16.

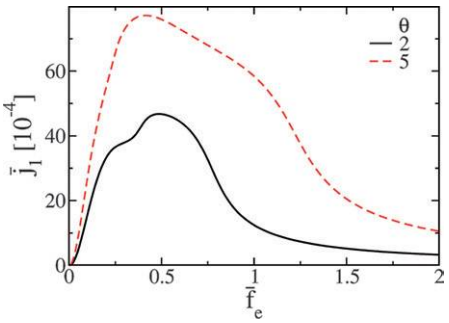

Fig. 18 The dependence of the flux on the external force for a type (iii) ratchet at the limit of large temporal periods, *i.e.*, neglecting transients during switching. Results are given for two flashing ratios (see legend). The parameters are $L = 32$, $\psi_i = 0$, $\varphi_i = 1$, $\mu = 1$, $\varepsilon = 0.75$, $A = 0.001$, $\bar{h} = 0.5$.

lies in the possibility of transporting entire droplets using appropriate temporal and spatial shifts, like $T/2$ and $L/2$, respectively. Fig. 16 gives two examples for such a transport. For sufficiently long flashing periods the system closely approaches the equilibrium state. This implies that most liquid is gathered near the point of highest wettability before the potential is switched. This can result in a nearly continuous transport of the droplets as in Fig. 16 (b). If, however, the flashing period is too short, virtually no liquid is transported. As illustrated in Fig. 16 (c), the droplets only slide back and forth in an oscillatory manner.

The transition between the continuous 'sliding' and 'oscillatory' regime is quite dramatic. Fig. 17 shows the dependence of the flux on the flashing period. One finds, for instance, that for flashing periods $T < 3000$ transport is extremely small (essentially only through the ultrathin wetting layer). However, it increases with the flashing period. For $T > 5000$ where droplets slide along as in Fig. 16 (b), transport is high but decreases with the flashing period. In between the two regimes the ratchet behavior is very complex. In the shaded region in Fig. 17 numerical simulations over 400 flashing cycles do not converge to a time-periodic behavior, indicating that the transition regime is highly unpredictable. To identify the optimal flux regime for practical applications will therefore require some fine-tuning. Despite this considerable drawback, note that the height of the flux maximum in dependence of the flashing period increases about 10 fold for $\bar{h} = 0.5$ [*cf.* Fig. 12 (b)]. For small and medium film thickness the transport direction is, as expected from the observations of the type (ii) ratchet, directed to the right. However, for large film thicknesses one observes a flux reversal and transport of liquid 1 is directed to the left ($\bar{h} = 0.7$ in Fig. 17). In this regime drops of liquid 1 are rather large and reach the dimensions of the spatial ratchet period. We conjecture that in this case it is the exact shape of the ratchet potential that is decisive for the transport direction. This question requires further studies.

4.4 Type (iii) ratchet—transport by a temporal asymmetry

It is known that even for systems with a reflection-symmetric periodic potential, transport can be induced by an asymmetry in the temporal driving (see ref. 70 and references therein). This is possible if the (asymmetric) stochastic forces exceed the (symmetric) deterministic forces. Here, we investigate the possibility of employing such a 'temporal ratchet' to transport fluid in the Stokes limit. A homogeneous external force is used that oscillates in time, but has a zero mean value. The exact definition is given in Section 2.1 as type (iii) ratchet. The temporal asymmetry is described by the flashing ratio θ [eqn (14)]. For $\theta = 1$ the oscillations in f_e are symmetric resulting in a zero mean flux.

In contrast to the type (i) and (ii) ratchets analysed up to here, we choose the most simple setting of a spatially homogeneous voltage, *i.e.*, $\psi_i = 0$, and $\varphi_i = 1$. To gain some understanding of this type of ratchet we first regard the limiting case of a large flashing period for the external force as compared to the intrinsic time scale of the film dynamics. Within this limit one may ignore transients due to the switching and assume that switching the force simply switches between two well known states of stationary sliding drops, as analysed, for instance, in ref. 58,71.

Fig. 18 gives the corresponding dependence of the flux on the magnitude of the external force. These results were obtained using continuation methods.[57] Obviously, for $\bar{f}_e = 0$ the flux is zero. However, increasing the external force from zero results in a non-zero flux. The flux is a direct consequence of the nonlinear relation between the sliding velocity of the droplets (or mean flow for a modulated film) and the external driving force (*e.g.*, *cf.* Fig. 7 in ref. 58). For large forces the flow decreases because the stationary solutions do not correspond to sliding drops anymore. A force dependent dynamic wetting transition leads to film flow modulated by surface waves.[58]

Identical fluxes as in Fig. 18 should be obtained for systems including transients, *i.e.*, in time simulations for finite temporal periods T, in the limit $T \to \infty$. Evidence is given in Fig. 19 that shows the dependence of the flux on a small RMS external force for various flashing periods. One can clearly see that the curve for $T = 10\,000$ has well approached the limiting curve that corresponds to $T \to \infty$. For all curves of Fig. 19 the flashing ratio is $\theta = 5$, *i.e.*, the absolute value of the external force is smaller in the first part of the flashing cycle than in the second. The force is positive in the first part of the cycle and negative in the second one. Taking this into account, the positive direction of the transport indicates that the slope of the curve $v(f_e)$ (mean velocity on external forcing) decreases with increasing f_e. This agrees well with results obtained for the velocity of droplets using, however, a different disjoining pressure (Fig. 7 in ref.

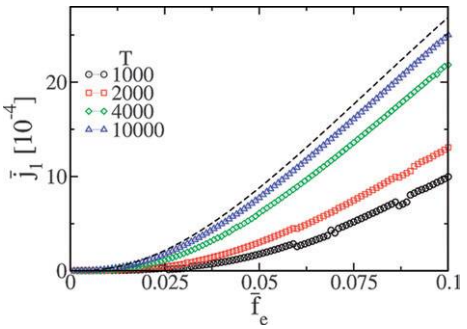

Fig. 19 The flux depending on the external force for different flashing periods as indicated in the legend [type (iii) ratchet]. The dashed line represents the flux for $T \to \infty$. Parameters are as in Fig. 18 with $\theta = 5$.

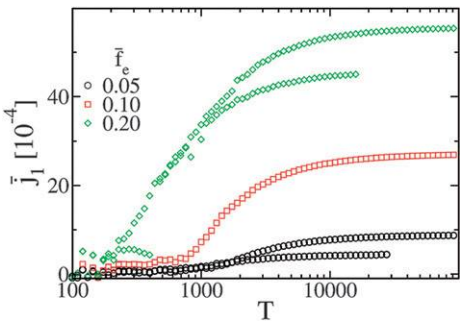

Fig. 20 The flux depending on the flashing period for different magnitudes of the external force as indicated in the legend [type (iii) ratchet]. Parameters are as in Fig. 18 with $\theta = 5$.

58). With increasing flashing period T the flux increases until it approaches the limiting value for infinitely large periods.

Studying next the dependence of the flux on the flashing period T we give in Fig. 20 corresponding curves for various values of the external force. For small periods one finds a rather unpredictable behavior of the ratchet because the flux is governed by transients. However, we see indications for the existence of a threshold value of T, that depends on the external force. Below the threshold the flux is negligible. For example, at $\bar{f}_e = 0.1$ the threshold is at $T \approx 800\ldots1000$.

Above the threshold the flux increases strongly with T and is clearly directed to the right. Curiously, results for the stationary regimes shown can depend strongly on the method that is used to arrive at the parameter values. Starting, for instance, at small flashing periods T, increasing T results in a smaller flux than starting with a stationary cycle with large T and decreasing T gradually. We emphasize that the two approaches result in two different *stationary cycles* beyond any transient. This intriguing hysteresis between different space- and time-periodic solutions for the same flashing ratchet system is related to the dynamic wetting transition with hysteresis discussed in ref. 58.

As before one can understand the dependencies regarding the limit $T \to \infty$, *i.e.*, ignoring transients due to switching: taking, for instance, Fig. 11 in ref. 58 one notices at intermediate driving forces a hysteresis between two stationary states corresponding to sliding droplets and small amplitude surface waves. The multi-valued stationary cycles found here can arise if one of the 'switching forces' ($\bar{f}_e/\sqrt{\theta}$ or $\bar{f}_e\sqrt{\theta}$) lies in the hysteresis region of the stationary states.

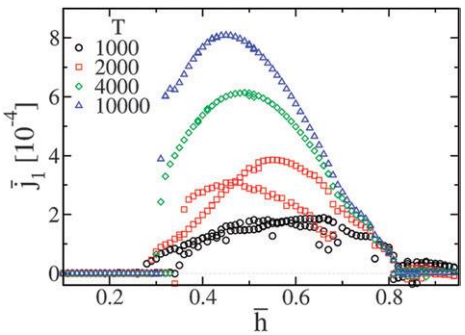

Fig. 21 The flux depending on the mean film thickness for different flashing periods as indicated in the legend [type (iii) ratchet]. The dashed line represents the flux for $T \to \infty$. Parameters are as in Fig. 18 with $\theta = 5$ and $\bar{f}_e = 0.05$.

Both, the threshold behavior and the multi-valuedness can also be appreciated in Fig. 21 giving the dependence of the flux on the mean film thickness. Here, the threshold behavior is very pronounced. For small film thicknesses below $\bar{h} \approx 0.35$ the flux is zero. The flat film is stable and the flux scales linearly with the external force (Poiseuille flow). Without nonlinearity in the force–velocity relation no transport can be generated. However, for thicker films the homogeneous film becomes unstable, the flux depends in a nontrivial nonlinear way on the force and transport is generated. Similar but less pronounced behavior is seen for thicker films at $\bar{h} \approx 0.8$. Note, finally, that the multi-valuedness is most pronounced for $T = 2000$ and could not be found at large T. This agrees well with the results given in Fig. 20 where one of the respective branches ends at some value of T.

5 Conclusions

We have presented a thin film model that allows us to study the behavior of a general class of 'wettability ratchets' in various specific settings. The objective has been to investigate the behavior of ratchets that can be used to transport a continuous medium in contrast to normally investigated ratchets that can be used to transport particles or molecules *within* a continuous carrier fluid without transporting the fluid.

After proposing the general model we have focused on an electrical dewetting mechanism based on the effective force a static electric field exercises on a liquid–liquid interface between two dielectric liquids. Out of the many ratchet types one can construct on this basis we have focused on (i) an on–off ratchet with a constant lateral force resulting in a dewetting–spreading cycle, (ii) a ratchet switching between two shifted potentials that shows a transition between oscillating and traveling drops, and (iii) a flashing, external force ratchet. We have shown that all of the proposed ratchet mechanisms can be used to produce a macroscopic transport in a liquid film with a free surface or in a two-layer system with a free interface. However, the characteristics of the transport vary strongly.

For a simple type (i) ratchet with a flashing asymmetric potential, we have identified the regimes of maximum transport by varying the spatial and temporal properties of the ratchet potential. It was found that transport can be generated with a high

reliability. For a given spatial form of the ratchet potential and combination of the liquid properties in the two layers the transport direction does not change, independent of the temporal switching of the ratchet or a variation in the proportions of the two liquids. On the one hand, this seems disappointing, since the direction of transport cannot be changed quickly, as required for some applications. On the other hand, however, this highly deterministic behavior does not require extensive fine-tuning to generate controlled directed transport.

For a one-layer ratchet, it had already been shown before,[27] that 5cS silicon oil is transported by the ratchet on time scales of 10 to 1×10^3 s, *i.e.*, the process is rather slow. Water, however, can be rapidly transported on time scales from 1×10^{-5} to 1×10^{-3} s. The advantage of the two-layer ratchet lies in the fact that the high permittivity and relatively low viscosity of water can be used to drive a liquid with a permittivity close to 1 and a high viscosity, as *e.g.* silicon oil. Re-visiting the time scales, one finds

$$t_0 = \frac{3\gamma\mu_s}{d\kappa_{el}} \sim \frac{\mu_s}{\varepsilon_s^2} \tag{27}$$

The quadratic dependence of the time scale on ε_s can be used to drive liquids of high viscosity but low permittivity. The increase of the effective viscosity μ_s is well compensated by the influence of ε_s. Note, that also very thin layers are effectively driven by the other (thick) layer. In this sense, a two-layer system is more versatile than a one-layer system.

An important advantage of the type (i) ratchet lies in the fact that the potential is switched off most of the time, since maximal transport was found for flashing ratios $\theta < 1$. This is an important issue if heating of the sample or a long exposure to an electric fields cause problems. However, for samples where this is not the case, transport can be sped up by utilizing a type (ii) ratchet, which switches between two shifted ratchet potentials. The latter permits transportation of entire droplets as individual entities whereas for a type (i) ratchet the dewetting–spreading cycle results in a flow of liquid through the droplets but not a motion of droplets. However, the more complex setup of a type (ii) ratchet, may also require a more extensive fine-tuning, because the transport direction depends even on the layer thicknesses in the capacitor.

In the last example we have explored a type (iii) ratchet that generates transport by switching the zero mean external force in an otherwise symmetric environment. Its working principle is based on a nonlinear dependence of flow or sliding velocity on the driving force, *i.e.*, it does not work for flat films. Indeed, it works very well in droplet or surface wave regimes. This effect can be used to generate transport in a reliable way, where the transport directions can be easily predicted. However, problems with predictability may be caused by hysteresis effects in parameter regions where the system allows for several stationary states like sliding drops and surface waves. In all cases studied, the hysteresis only affects the magnitude of the flux, but not its direction. A physical realization of the external force could be a time-dependent, macroscopic pressure gradient or a time-periodic variation of the inclination angle of the substrate. In contrast, droplets on substrates with a global wettability gradient move under vibration[16,17] not because of a ratchet effect, but because the vibration facilitates depinning at local heterogeneities. In other words, there the transport is induced directly by the substrate asymmetry, whereas the external force of the type (iii) ratchet directly fuels the transport. No local or global substrate asymmetry is necessary.

In conclusion, we have proposed a physical system that allows to investigate an entire 'toolbox' of ratchets. All of them generate transport of small liquid volumes on small scales on feasible time scales.

Acknowledgements

This work was supported by the European Union and Deutsche Forschungsgemeinschaft under grants MRTN-CT-2004-005728 and SFB 486, project B13, respectively. K. J. was supported by grants from the CNES and the Humboldt-Foundation and P. H. thanks the German Excellence Initiative *via* the Nanosystems Initiative Munich (NIM).

References

1 R. D. Astumian, *Science*, 1997, **276**, 917–922.
2 R. D. Astumian and P. Hänggi, *Phys. Today*, 2002, **55**(11), 33.
3 P. Reimann and P. Hänggi, *Appl. Phys. A: Mater. Sci. Process.*, 2002, **75**, 169.
4 P. Hänggi, F. Marchesoni and F. Nori, *Ann. Phys.-Berlin*, 2005, **14**, 51.
5 J. Rousselet, L. Salomé, A. Ajdari and J. Prost, *Nature*, 1994, **370**, 446–448.
6 F. Müller, A. Birner, J. Schilling, U. Gosele, C. Kettner and P. Hanggi, *Phys. Status Solidi A*, 2000, **182**, 585.
7 C. Kettner, P. Reimann, P. Hänggi and F. Müller, *Phys. Rev. E*, 2000, **61**, 312.
8 S. Matthias and F. Müller, *Nature*, 2003, **424**, 53.
9 F. Jülicher, A. Ajdari and J. Prost, *Rev. Mod. Phys.*, 1997, **69**, 1269.
10 P. Curie, *J. Phys. (Paris)*, 1894, **III**, 383.
11 A. Engel, H. W. Müller, P. Reimann and A. Jung, *Phys. Rev. Lett.*, 2003, **91**, 060602.
12 A. D. Stroock, R. F. Ismagilov, H. A. Stone and H. M. Whitesides, *Langmuir*, 2003, **19**, 4358.
13 D. Queré and A. Ajdari, *Nat. Mater.*, 2006, **5**, 429.
14 H. Linke, B. J. Aleman, L. D. Melling, M. J. Taormina, M. J. Francis, C. C. Dow-Hygelund, V. Narayanan, R. P. Taylor and A. Stout, *Phys. Rev. Lett.*, 2006, **96**, 154502.
15 A. Buguin, L. Talini and P. Silberzan, *Appl. Phys. A: Mater. Sci. Process.*, 2002, **75**, 207.
16 S. Daniel and M. K. Chaudhury, *Langmuir*, 2002, **18**, 3404.
17 S. Daniel, S. Sircar, J. Gliem and M. K. Chaudhury, *Langmuir*, 2004, **20**, 4085.
18 P. Jung, J. G. Kissner and P. Hänggi, *Phys. Rev. Lett.*, 1996, **76**, 3436.
19 B. Lindner, L. Schimansky-Geier, P. Reimann, P. Hänggi and M. Nagaoka, *Phys. Rev. E*, 1999, **59**, 1417.
20 H. Chen, Q. Wang and Z. Zheng, *Phys. Rev. E*, 2005, **71**, 031102.
21 L. Schimansky-Geier, M. Kschischo and T. Fricke, *Phys. Rev. Lett.*, 1997, **79**, 3335.
22 G. M. Whitesides and A. D. Stroock, *Phys. Today*, 2001, **54**(6), 42.
23 H. A. Stone, A. D. Stroock and A. Ajdari, *Annu. Rev. Fluid Mech.*, 2004, **36**, 381.
24 T. M. Squires and S. R. Quake, *Rev. Mod. Phys.*, 2005, **77**, 977.
25 A. Ajdari, *Phys. Rev. E*, 2000, **61**, R45.
26 A. Ramos, H. Morgan, N. G. Green, A. Gonzales and A. Castellanos, *J. Appl. Phys.*, 2005, **97**, 084906.
27 K. John and U. Thiele, *Appl. Phys. Lett.*, 2007, **90**, 264102.
28 Z. Q. Lin, T. Kerle, S. M. Baker, D. A. Hoagland, E. Schäffer, U. Steiner and T. P. Russell, *J. Chem. Phys.*, 2001, **114**, 2377.
29 Z. Q. Lin, T. Kerle, T. P. Russell, E. Schäffer and U. Steiner, *Macromolecules*, 2002, **35**, 3971.
30 D. Merkt, A. Pototsky, M. Bestehorn and U. Thiele, *Phys. Fluids*, 2005, **17**, 064104.
31 G. Reiter, *Phys. Rev. Lett.*, 1992, **68**, 75–78.
32 S. Herminghaus, K. Jacobs, K. Mecke, J. Bischof, A. Fery, M. Ibn-Elhaj and S. Schlagowski, *Science*, 1998, **282**, 916.

33 U. Thiele, M. Mertig and W. Pompe, *Phys. Rev. Lett.*, 1998, **80**, 2869–2872.
34 U. Thiele, M. G. Velarde, K. Neuffer, M. Bestehorn and Y. Pomeau, *Phys. Rev. E*, 2001, **64**, 061601.
35 J. Becker, G. Grün, R. Seemann, H. Mantz, K. Jacobs, K. R. Mecke and R. Blossey, *Nature Mat.*, 2003, **2**, 59–63.
36 E. Schäffer, T. Thurn-Albrecht, T. Russell and U. Steiner, *Europhys. Lett.*, 2001, **53**, 518.
37 M. D. Morariu, N. E. Voicu, E. Schäffer, Z. Q. Lin, T. P. Russell and U. Steiner, *Nat. Mater.*, 2003, **2**, 48.
38 R. Verma, A. Sharma, K. Kargupta and J. Bhaumik, *Langmuir*, 2005, **21**, 3710–3721.
39 D. Bandyopadhyay and A. Sharma, *J. Colloid Interface Sci.*, 2007, **311**, 595–608.
40 A. Pototsky, M. Bestehorn, D. Merkt and U. Thiele, *Phys. Rev. E*, 2004, **70**, 025201(R).
41 A. Pototsky, M. Bestehorn, D. Merkt and U. Thiele, *Europhys. Lett.*, 2006, **74**, 665–671.
42 R. Konnur, K. Kargupta and A. Sharma, *Phys. Rev. Lett.*, 2000, **84**, 931–934.
43 K. Kargupta, R. Konnur and A. Sharma, *Langmuir*, 2000, **16**, 10243–10253.
44 L. Brusch, H. Kühne, U. Thiele and M. Bär, *Phys. Rev. E*, 2002, **66**, 011602.
45 U. Thiele, L. Brusch, M. Bestehorn and M. Bär, *Eur. Phys. J. E*, 2003, **11**, 255.
46 K. Kargupta and A. Sharma, *Phys. Rev. Lett.*, 2001, **86**, 4536.
47 A. Oron, S. H. Davis and S. G. Bankoff, *Rev. Mod. Phys.*, 1997, **69**, 931.
48 *Thin Films of Soft Matter*, ed. S. Kalliadasis and U. Thiele,Springer, Wien, 2007.
49 D. Merkt, A. Pototsky, M. Bestehorn and U. Thiele, *Phys. Fluids*, 2005, **17**, 064104.
50 P.-G. de Gennes, *Rev. Mod. Phys.*, 1985, **75**, 827.
51 J. N. Israelachvili, *Intermolecular and Surface Forces*, Academic Press, London, 1992.
52 L. Machura, M. Kostur, P. Talkner, J. Luczka, F. Marchesoni and P. Hänggi, *Phys. Rev. E*, 2004, **70**, 061105.
53 L. Machura, M. Kostur, F. Marchesoni, P. Talkner, P. Hänggi and J. Luczka, *J. Phys.: Condens. Matter*, 2005, **17**, S3741.
54 L. Machura, M. Kostur, F. Marchesoni, P. Talkner, P. Hänggi and J. Luczka, *J. Phys.: Condens. Matter*, 2006, **18**, 4111.
55 E. Doedel, H. B. Keller and J. P. Kernevez, *Int. J. Bifurcation Chaos Appl. Sci. Eng.*, 1991, **1**, 493.
56 E. Doedel, H. B. Keller and J. P. Kernevez, *Int. J. Bifurcation Chaos Appl. Sci. Eng.*, 1991, **1**, 745.
57 E. J. Doedel, A. R. Champneys, T. F. Fairgrieve, Y. A. Kuznetsov, B. Sandstede, and X. J. Wang, *AUTO97: Continuation and Bifurcation Software for Ordinary Differential Equations*, Concordia University, Montreal, 1997.
58 U. Thiele, M. G. Velarde, K. Neuffer, M. Bestehorn and Y. Pomeau, *Phys. Rev. E*, 2001, **64**, 061601.
59 U. Thiele and E. Knobloch, *Physica D*, 2004, **190**, 213.
60 K. John, M. Bär and U. Thiele, *Eur. Phys. J. E*, 2005, **18**, 183.
61 U. Thiele and E. Knobloch, *New J. Phys.*, 2006, **8**, 313.
62 A. Pototsky, M. Bestehorn, D. Merkt and U. Thiele, *J. Chem. Phys.*, 2005, **122**, 224711.
63 V. S. Mitlin, *J. Colloid Interface Sci.*, 1993, **156**, 491–497.
64 U. Thiele, M. Velarde, K. Neuffer and Y. Pomeau, *Phys. Rev. E*, 2001, **64**, 031602.
65 U. Thiele, K. Neuffer, Y. Pomeau and M. G. Velarde, *Colloids Surf., A*, 2002, **206**, 135–155.
66 K. Kargupta and A. Sharma, *J. Colloid Interface Sci.*, 2002, **245**, 99.
67 K. Kargupta and A. Sharma, *Langmuir*, 2003, **19**, 5153.
68 M. Brinkmann and R. Lipowsky, *J. Appl. Phys.*, 2002, **92**, 4296.
69 W. H. Press, S. A. Teukolsky, W. T. Vetterling and B. P. Flannery, *Numerical Recipes in C*, Cambridge University Press, Cambridge, 2002.
70 P. Hänggi, R. Bartussek, P. Talkner and J. Luczka, *Europhys. Lett.*, 1996, **35**, 315.
71 U. Thiele, K. Neuffer, M. Bestehorn, Y. Pomeau and M. G. Velarde, *Colloids Surf., A*, 2002, **206**, 87–104.